Effects of gliding arc discharge penetrating a premixed flame

Jiajian Zhu[1], Andreas Ehn[1], Jinlong Gao[1], Marcus Aldén[1], Zhongshan Li[*, 1]

Tomas Hurtig[2], Anders Larsson[2] and Yukihiro Kusano[3]

[1]Division of Combustion Physics, Lund University, P.O. Box 118, S-221 00 Lund, Sweden
[2]Swedish Defence Research Agency, SE-164 90 Stockholm, Sweden
[3]Department of Wind Energy, Section for Composites and Materials Mechanics, Technical University of Denmark, Risø Campus, Frederiksborgvej 399, DK-4000 Roskilde, Denmark

Abstract

In this work, a reactor integrating gliding arc discharges with a premixed air/CH_4 flame is built to allow the plasma column to penetrate the flame. Interactions between the gliding arc discharge and the premixed flame are studied using both electrical and optical diagnostics. Influences of flames on the gliding arc discharge are investigated using simultaneous measurements of current, voltage and high-speed images; while effects of the gliding arc on the premixed flames are studied using planar laser-induced fluorescence of hydroxyl radicals (OH) and formaldehyde (CH_2O). The flame was discovered to facilitate the ignition process of the gliding arc discharge with more frequent ignitions and lift the ignition position. The gliding arc discharge was observed to pass through the flame, and promote OH and CH_2O formation in the flame. The preliminary results call for further experimental studies and modelling for a better understanding of the mechanism and kinetics of the interactions between the gliding arc discharge and the premixed flame.

Introduction

Plasma-assisted combustion (PAC) has attracted growing interest for the potential applications in gas turbine, ultra-lean combustor, internal combustion engine and scramjets [1, 2]. Much attention has been paid to study PAC and understand PAC-related kinetics. One way to study PAC is to deliver active species, which can be generated by plasmas, into the flame. Effects of active species like O_3 and O_2 ($a_1\Delta g$) on the flames have been experimentally and numerically studied [3-5]. Another way to investigate PAC is to directly couple electric energy of plasmas to flames. The potential plasma sources for PAC include microwave discharge [6, 7], dielectric barrier discharge (DBD) [8, 9], gliding arc (GA) discharge [10, 11].

Gliding arc discharge is advantageous for its simplicity to generate low temperature plasmas and easy operations in atmospheric pressure air [12]. In order to investigate the feasibility of PAC using gliding arc, optical and electrical diagnostics of gliding arc discharge were performed to understand the discharge behaviors [13-17]. The gliding arc discharge is able to produce a sustained diffusive non-thermal plasma column at a large volume and high power [14], and generate a large number of active species in open air, e.g. OH^*, NO^*, N_2^* [13, 16]. Previous works studied the effect of gliding arc discharges at low air temperature on a diffusion flame, showing a significant increase in the extinction strain rate by thermal effects [10, 11]. Apart from the above-mentioned work, detailed investigations of interactions between gliding arc discharge and flames, especially premixed flames have not been reported.

In this paper, a reactor integrating a gliding arc discharge and a premixed flame was built, and interactions between the discharge and the flame were studied using electrical and optical diagnostics, including current and voltage measurements, high-speed imaging, and planar laser-induced fluorescence (PLIF).

Experimental setup

Figure 1 shows the experimental setup of the discharge system, and the electrical and optical diagnostics system. The discharge system is depicted in Fig. 1(a). The gliding arc discharge was generated at the gap between two diverging knife-shaped electrodes. One of the electrodes was connected to a 35 kHz AC power supply (Generator 9030E, SOFTAL Electronic GmbH) while the other was grounded. An air flow or air/CH_4 mixture was ejected through a nozzle between the two electrodes to extend the generated plasma column upwards. Three different flows listed in Table. 1 were used in the experiment to achieve different operating conditions of the gliding arc discharge (GA I, GA II, GA III). In GA I, 4.8 Standard Liter per Minute (SLM) pure air was used as working gas; In GA II,

*. Corresponding author: zhongshan.li@forbrf.lth.se

a premixed air/CH_4 mixture (4.8 SLM air and 0.3 SLM CH_4) was employed and the mixture is too lean (Φ is about 0.6) to ignite a flame; in GA III, a premixed mixture with 4.8 SLM air and 0.6 SLM CH_4 was fed to the discharge system, and a gliding arc discharge and a premixed flame with a stoichiometric ratio of about 1.2 can simultaneously exist.

The electrical diagnostics system is also shown in Fig. 1(a). A current monitor (Pearson Electronics) and a voltage probe (Tektronix P6015A) were used to measure current and voltage waveforms. The current and voltage were recorded by a four-channel oscilloscope (PicoScope 4424). A high framing-speed camera (Phantom v7.1) mounted with an objective lens (Nikon, 100 mm, f/2.8) was employed to simultaneously capture snap shot images of the gliding arc discharge with the recording current and voltage. Measurements of high-speed observations were performed at a frame rate of 10 kHz with an exposure time of 20 μs and a resolution of 512×384 pixels. The high-speed camera and the oscilloscope were externally triggered by a pulse generator (BNC 575) in order to simultaneously record the data.

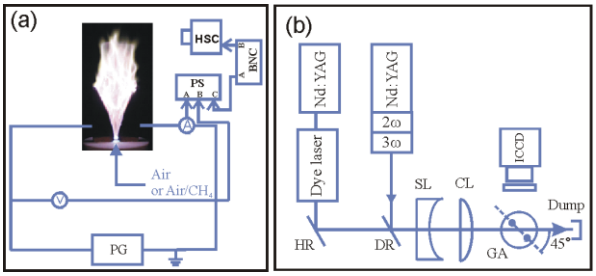

Fig. 1 (a) Schematic of the experimental setup for simultaneous measurements of current, voltage and high-speed images. PG: power generator; PS: 4-channels picoscope; BNC: trigger pulse generator; HSC: high-speed camera. (b) Experimental arrangement for OH and CH_2O PLIF measurements

The experimental setup of PLIF measurements is illustrated in Fig. 1(b). For the OH-PLIF measurements, a Nd:YAG-pumped dye laser (Cobra Stretch-G-2400, Sirah), using Rhodamine 610, was frequency-doubled to 308.717 nm. The laser beam was operated at about 4 mJ per pulse. For the CH_2O PLIF measurements, a 150 mJ per pulse frequency-tripled Nd:YAG laser (Brilliant b) with a wavelength of 355 nm was used. The OH and CH_2O were performed separately. The laser beam was directed to a cylindrical lens (CL, f = -40 mm) and a spherical lens (SL, f = 500 mm for OH measurement, f = 200 mm for CH_2O measurement) by a dichroic mirror (DR) and formed a vertically oriented laser sheet. The laser sheet was sent through the electrodes at an angle of 45° to the plane containing the two electrodes. The fluorescence was detected by an ICCD camera (Princeton PI-MAX I) mounted with an objective lens (B. Halle Nachfl, 100 mm, f/2) and a filter (Semrock, 40 nm bandwidth centered at 320 nm for OH measurement; WG 395 for CH_2O measurements).

Table. 1 Scheme of flows for the gliding arc (GA) discharge and flame

	GA I	GA II	GA III
Air (SLM)	4.8	4.8	4.8
CH_4 (SLM)	0	0.3	0.6
Conditions	Only GA	Only GA	Flame and GA

Results and discussion

Figure 2 shows photos of the premixed flame, GA I and GA III. The photos were recorded by a digital camera (Cannon 650D) with an exposure time of 1/30 s. Figure 2(a) displays a premixed flame stabilized between the two diverging electrodes. Figure 2(b) shows the gliding arc discharge generated at the narrowest gap of the two electrodes in the pure air while Fig. 2(c) shows that the discharge in presence of the premixed flame where the discharge with shorter plasma columns is ignited at higher and wider position. Emission from the discharge dominates in Fig. 2(c) and therefore the flame emission is not obvious. However, in Fig. 2(c) , the flame can be still seen at the bottom of the electrodes where the discharge is absent.

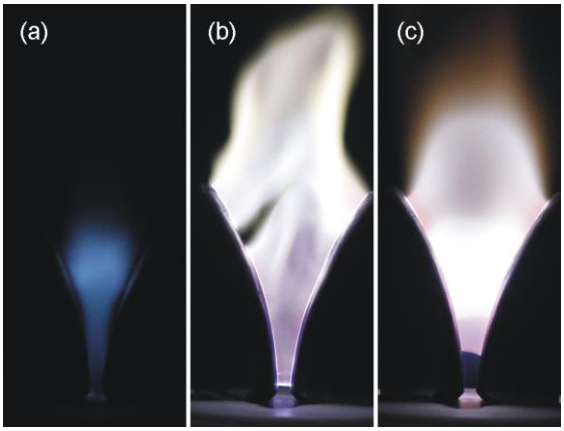

Fig. 2 Photos of flame and/or the gliding arc discharge with an exposure time of 1/30 s. (a) Premixed flame; (b) GA I; (c) GA III. The Φ for the flame is about 1.2. In GA I, the gliding arc discharge was operated in pure air. in GA III, the

working gas is premixed air/CH_4 mixture where the discharge penetrates into a premixed flame.

Fig. 3(a) and 3(b) show the current and voltage waveform of GA I and GA III during a 300 ms time span, respectively. With the presence of the flame in GA III, the current and voltage waveform of the gliding arc discharge differ significantly compared with GA I without a flame: (*i*) smaller current and voltage spikes are observed in GA III; (*ii*) more oscillation periods of the current and voltage envelope occur in GA III. Detailed current and voltage waveform for the marked period are shown in Fig. 4.

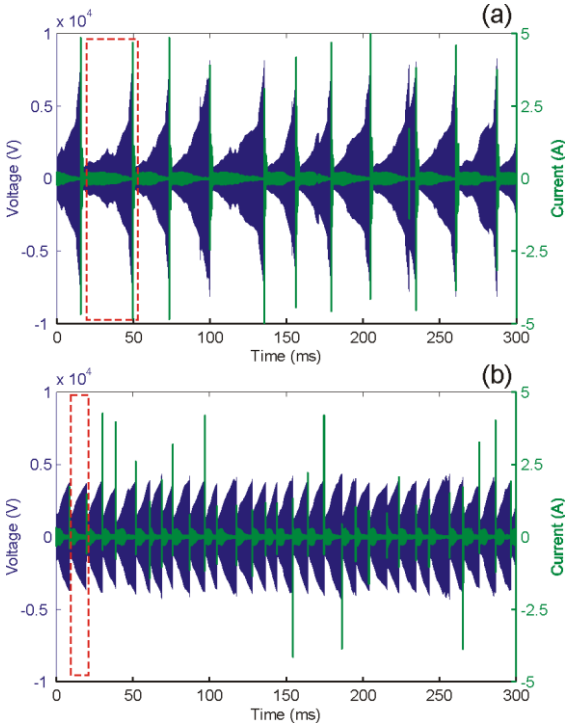

Fig. 3 Current and voltage waveforms of the gliding arc discharge during a 300 ms time span. (a) GA I and (b) GA III. Detailed current and voltage waveforms for the marked period (by a red square) are shown in Fig. 4.

Figure 4 shows the current and voltage waveforms for the oscillation period marked in Fig. 3. The oscillation period in GA I is about 35 ms while that in GA III is about 12 ms. The period starts at the time t1 or T1 where the largest current and the smallest voltage are observed. The voltage generally increases over the period, and the current decreases due to the rated output power of the power supply. The detailed current and voltage waveform during a 0.1 ms time span is shown as an insert in Fig. 4 where the sinusoidal-like waveform can be seen. The period of the sinusoidal-like waveform is about 28 μs, corresponding to the driving signal of the power supply (35 kHz). The current and voltage measurements are synchronized with the instantaneous observation of the GA I and GA III recorded by the high-speed camera, which are shown in Fig. 5.

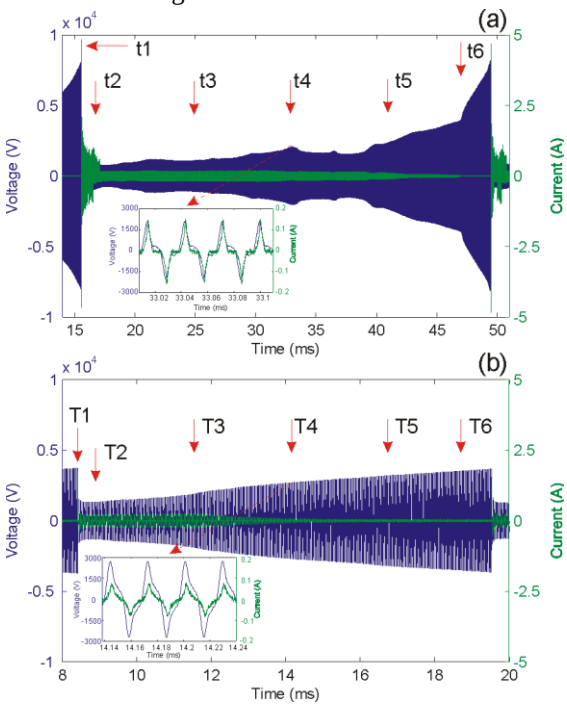

Fig. 4 Current and voltage waveforms of the gliding arc discharge for the marked oscillation period in Fig. 3. (a) GA I and (b) GA III. Detailed current and voltage waveforms during a 0.1 ms time span are shown as inserts.

The instantaneous images of the GA I and GA III recorded by the high-speed camera at the time points t1~t6 and T1~T6 are shown in Fig. 5 as well as the typical frames of the flame emission. In Fig. 5(a), several typical frames of the premixed flame are observed between the two diverging electrodes. The flame exhibits various flame shapes in the turbulent regime where the Reynolds number (Re) at the nozzle exit is around 3200. Fig. 5(b) shows images of GA I where the discharge is ignited at the narrowest gap of the two electrodes at time t1. The corresponding ignition voltage shown in Fig. 4(a) is 8.2 kV. The afterglow still exists at the top of the electrodes when the ignition occurs. After the ignition, the newly ignited plasma column surrounded by the emissions from active species elongates upwards as the afterglow gradually fades away. During the elongation of the plasma column, the voltage is increasing. Similar phenomena were found in previous works by Zhu et al. [13, 14]. For GA III, shown in Fig. 5(c), the plasma column and

the flame are simultaneously seen, and the plasma column passes through the flame. The elongation of the plasma column and the increase of the voltage, which was recognized in GA I, can also be found in GA III. However, different phenomena in GA III are observed: (*i*) the plasma column in the GA III is ignited at wider gap, which was also observed in Fig. 2; (*ii*) the plasma column in GA III becomes more diffusive when it penetrates into the flame.

The different ignition position may be resulted from the higher temperature in GA III where the flame is present. The higher temperature (T) will lead to lower number density (N) and further result in larger reduced electric field strength (E/N). Due to the increase of reduced electric field strength, the discharge is much easier to be ignited in GA III and re-ignitions of the gliding arc discharge are observed more frequently. The wider plasma column in the flame may be due to the chemical reactions of the active species generated in the flame although detailed kinetic processes are still unclear.

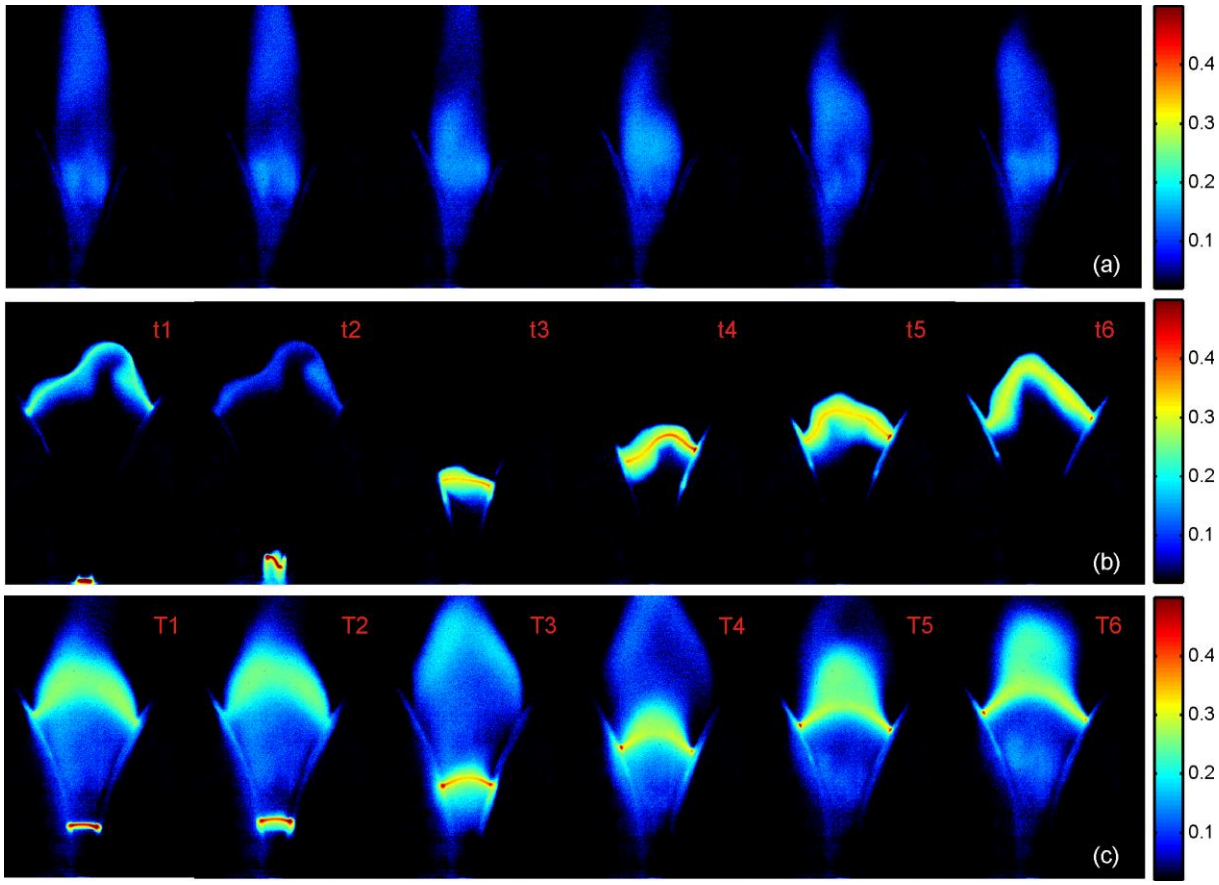

Fig. 5 Instantaneous images recorded by the high-speed camera (a) Flame; (b) GA I; (c) GA III. The time points t1~t6 and T1~T6 were labeled in the current and voltage waveform in Fig. 4.

Figure 6 shows OH-PLIF images with a 50 ns exposure time. Averaged OH distributions in the flame are displayed in Fig. 6(a) while Fig 6(b), 6(c) and 6(d) show the single-shot OH distributions in GA I, GA III and GA II, respectively. The the OH distribution with a ring structure in GA I was previously reported [13, 16]. In the presence of a flame as shown in Fig. 6(c), the ring structure of OH distributions still exists but the intensity of the OH signal becomes stronger. It is believed that the stronger OH signal is primarily due to the reactions between the discharge, CH_4 and O_2 although detailed reaction pathways are still unknown. This can be concluded from Fig. 6(d) where 0.3 SLM CH_4 and 4.8 SLM air was supplied into the discharge system and the mixtures are too lean to ignite a flame, showing that the OH signal in GA II also becomes stronger than that in GA I.

Fig. 7 illustrates single-shot OH-PLIF images for GA I, GA II and GA III where a 2 μs exposure time is used to simultaneously show OH distributions and the plasma column. The OH is distributed in the surrounding area of the plasma column and the plasma column passed through the core of the OH signals as shown in Fig. 7(a) and 7(c). In the GA III shown in Fig. 7(b), the hollow core of the OH signal is not obvious due to the strong emission from the plasma column and the

flame. Besides, in Fig. 7(b) where the flame is present, the plasma column is also thicker and stronger in the emission intensity.

Figure 8 shows CH_2O distributions in the flame, GA III and GA II in (a), (b) and (c), respectively. The images were obtained by accumulating 200 single-shot CH_2O PLIF images. Note that there is no CH_2O signal in GA I since it is operated in pure air. In presence of the discharge and the flame (see Fig. 8(b)), the CH_2O is distributed in shorter but wider area than that only in the flame shown in Fig. 8(a). Besides, the intensity of the CH_2O signal is almost kept at the same level. Fig. 8(c) shows CH_2O distributions in GA II where the gliding arc discharge was operated at the lean air/CH_4 mixture without a flame. The CH_2O distributions are much stronger and distributed at a much wider area than those shown in Fig. 8(a) and Fig. 8(b). It can be concluded from Fig. 8(b) and Fig. 8(c) that the gliding arc discharge in the air/CH4 mixture can form CH_2O and the CH_2O may be consumed in the presence of a flame. The mechanism of the CH_2O formation and consumption are required for further investigation.

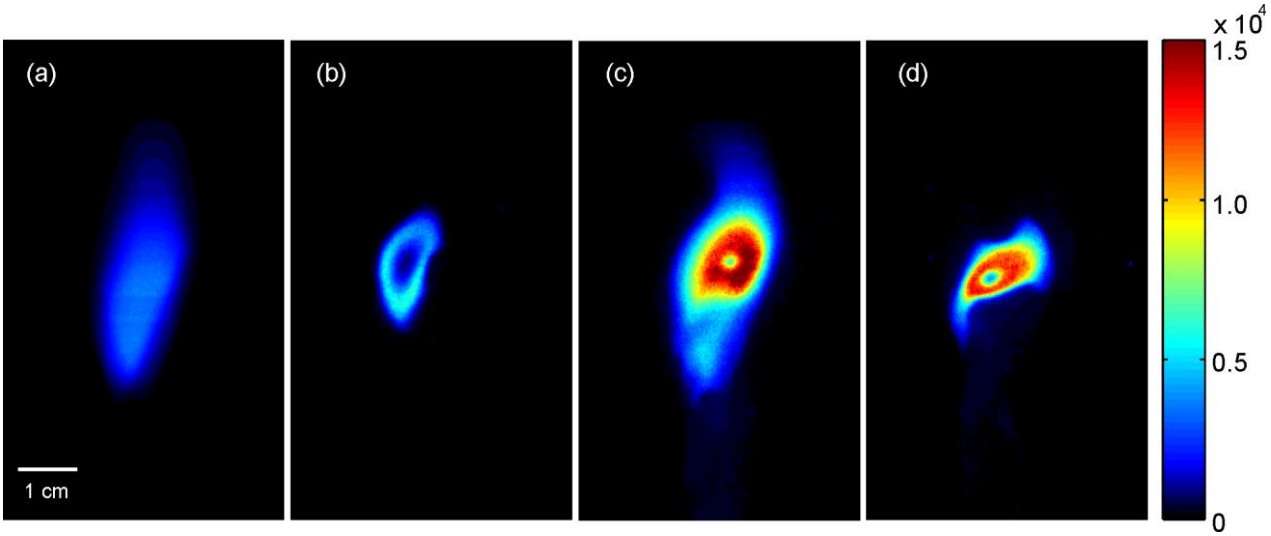

Fig.6 OH-PLIF images (a) Flame; (b) GA I; (c) GA III; (d) GA II. Fig. 6(a) is an averaged image while the others are single-shot images. Exposure time is 50 ns.

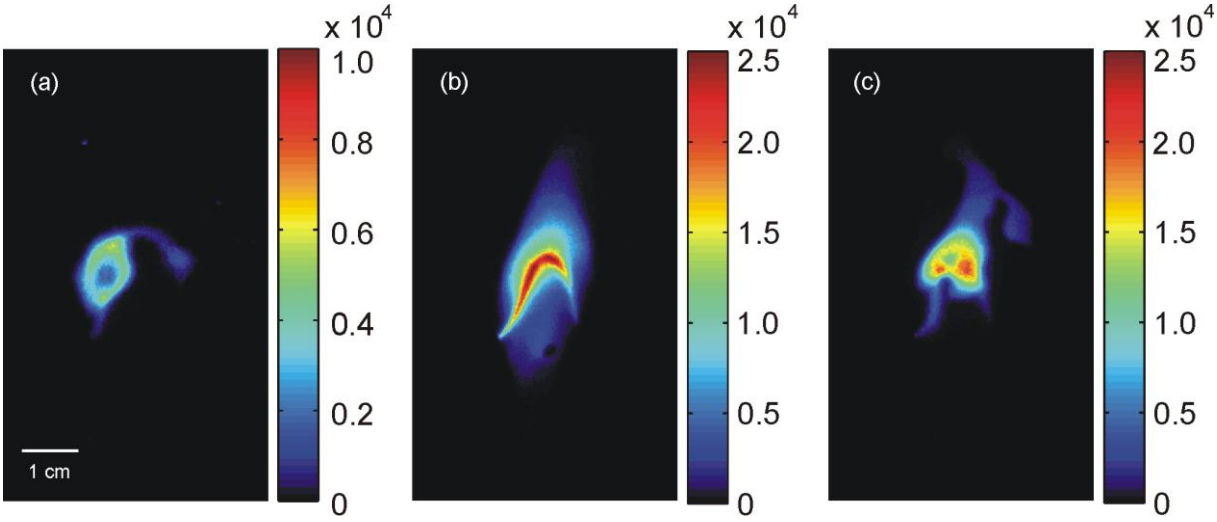

Fig. 7 Single-shot OH-PLIF images. (a) GA I; (b) GA III; (c) GA II. An exposure time of 2 μs was used to simultaneously record the plasm column with the OH distributions.

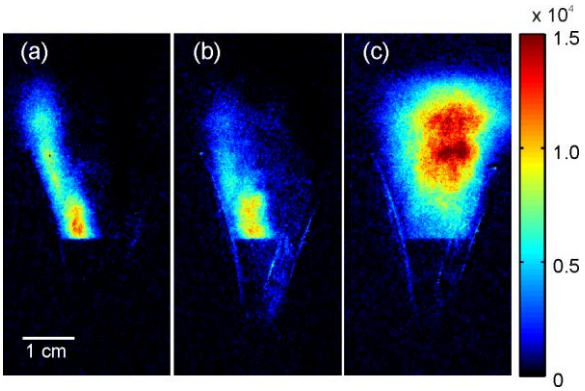

Fig. 8 CH_2O-PLIF images. (a) Flame; (b) GA III; (c) GA II. 200 single-shot CH_2O PLIF images are accumulated.

Conclusion

Interactions between the gliding arc discharge and the premixed flame were experimentally investigated using electric diagnostics, high-speed imaging and PLIF measurements.

Electric diagnostics shows that the flame not only facilitates ignition processes of the gliding arc discharge, but also reduces the ignition voltage.

High-speed imaging shows that the plasma column can penetrate and pass through the flame. The presence of the flame in the gliding arc discharge will lift the ignition position between the two electrodes and make the plasma column more diffusive and thicker.

OH-PLIF measurements show that the gliding arc discharge promotes OH formation in the flame mostly due to the reactions between the plasma column and the air/CH_4 mixture. Formaldehyde-PLIF measurements suggest that the gliding arc discharge changes the shapes of the CH_2O in the flame and the CH_2O signal can be significantly enhanced by the gliding arc discharge in lean air/CH_4 mixture. The detailed mechanisms for the formations and consumptions of OH and CH_2O in the flame and the discharge are required for further experimental studies and modeling.

Interactions between the gliding arc discharge and the premixed flame are complex and further investigations are necessary for a better and deepened understanding of the fundamental mechanism and chemical kinetics.

Acknowledgements

The work was financially supported by the Swedish Energy Agency, the Knut & Alice Wallenberg Foundation, the Swedish Research Council and the European Research Council. J. Zhu would like to thank the Chinese Scholarship Council for financial support.

References

[1]. Y. Ju; W. Sun, Prog. Energ, Combust. 48 (2015) 21-83.
[2]. S. M. Starikovskaia, J Phys D Appl Phys 39 (16) (2006) R265-R299.
[3]. T. Ombrello; S. H. Won; Y. G. Ju; S. Williams, Combustion and Flame 157 (10) (2010) 1906-1915.
[4]. T. Ombrello; S. H. Won; Y. G. Ju; S. Williams, Combustion and Flame 157 (10) (2010) 1916-1928.
[5]. A. Ehn; J. J. Zhu; P. Petersson; Z. S. Li; M. Aldén; C. Fureby; T. Hurtig; N. Zettervall; A. Larsson; J. Larfeldt, Proceedings of the Combustion Institute (0)).
[6]. C. Wang; W. Wu, Combustion and Flame 161 (8) (2014) 2073-2084.
[7]. K. W. Hemawan; C. L. Romel; S. Zuo; I. S. Wichman; T. A. Grotjohn; J. Asmussen, Appl. Phys. Lett. 89 (14) (2006).
[8]. A. Vincent-Randonnier; S. Larigaldie; P. Magre; V. Sabel'nikov, Plasma Sources Sci. T. 16 (1) (2007) 149-160.
[9]. Y. Matsubara; K. Takita; G. Masuya, Proceedings of the Combustion Institute 34 (2013) 3287-3294.
[10]. T. Ombrello; X. Qin; Y. G. Ju; C. Carter, AIAA Journal 44 (1) (2006) 142-150.
[11]. A. Fridman; A. Gutsol; S. Gangoli; Y. G. Ju; T. Ombrellol, J. Propul. Power 24 (6) (2008) 1216-1228.
[12]. A. Fridman; S. Nester; L. A. Kennedy; A. Saveliev; O. Mutaf-Yardimci, Prog. Energ, Combust. 25 (2) (1999) 211-231.
[13]. J. Zhu; Z. Sun; Z. Li; A. Ehn; M. Aldén; M. Salewski; F. Leipold; Y. Kusano, J. Phys. D: Appl. Phys. 47 (29) (2014) 295203.
[14]. J. Zhu; J. Gao; Z. Li; A. Ehn; M. Aldén; A. Larsson; Y. Kusano, Appl. Phys. Lett. 105 (23) (2014) 234102.
[15]. J. Zhu; J. Gao; A. Ehn; M. Aldén; Z. Li; D. Moseev; Y. Kusano; M. Salewski; A. Alpers; P. Gritzmann; M. Schwenk, Appl. Phys. Lett. 106 (4) (2015) -.
[16]. Z. W. Sun; J. J. Zhu; Z. S. Li; M. Aldén; F. Leipold; M. Salewski; Y. Kusano, Opt. Express 21 (5) (2013) 6028-6044.
[17]. A. Larsson; L. Adelöw; M. Elfsberg; T. Hurtig, IEEE Trans. Plasma Sci. 42 (10) (2014) 3186-3190.